


Broadband Electromagnetic Wave Tunneling with Transmuted Material Singularity

Yichao Liu,¹ Fei Sun^{1,*}, Yibiao Yang,¹ Zhihui Chen,¹ Jianzhong Zhang¹, Sailing He,^{2,3} and Yungui Ma^{2,†}

¹Key Lab of Advanced Transducers and Intelligent Control System, Ministry of Education and Shanxi Province, College of Physics and Optoelectronics, Taiyuan University of Technology, Taiyuan 030024 China

²State Key Lab of Modern Optical Instrumentation, Centre for Optical and Electromagnetic Research, College of Optical Science and Engineering; International Research Center for Advanced Photonics, Zhejiang University, Hangzhou 310058 China

³Department of Electromagnetic Engineering, School of Electrical Engineering, Royal Institute of Technology (KTH), S-100 44 Stockholm, Sweden

 (Received 26 May 2020; revised 5 October 2020; accepted 13 October 2020; published 10 November 2020)

Subwavelength channels filled with near-zero-index (NZI) media can realize extraordinary optical functionalities, for example, tunneling electromagnetic wave without reflections, but usually confined in a narrow wavelength band due to the material singularity (refractive index $n \approx 0$), which seriously limits the practical potentials. In this Letter, we show this limit can be fundamentally overcome by an alternative, named near-zero-index-featured (NZIF) structure, with the singularity transmuted via a controlled optical conformal mapping, enabling the device implementation with nonmagnetic normal dielectrics (i.e., relative permittivity > 1). Their equivalence is strictly examined through a subwavelength tunneling waveguide. Classic wave tunneling features in a broad frequency range are revealed in various confined geometries. These properties are robust against the disturbance of several kinds of structural defects benefited from the infinite effective local wavelength. The broadband and lossless NZIF medium proposed here provides a promising way to pursue the fascinating light controlling functionalities as initially enabled by singular NZI materials.

DOI: [10.1103/PhysRevLett.125.207401](https://doi.org/10.1103/PhysRevLett.125.207401)

Near-zero-index (NZI) materials can give birth to many interesting electromagnetic phenomena, including electric-magnetic field decoupling, diverging velocities, and wavelength expansion, etc. [1,2], which endow them with unprecedented measures in controlling light and waves with prominent functionalities, such as photon tunneling [3–9], light trapping [10,11], directive emission [12–16], or extreme nonlinear interactions [17–20]. Among them, reflectionless light tunneling through subwavelength channels has attracted particular attention for the potential application in transmitting light signals [3–7]. So far, several methods have been proposed to realize NZI media, such as using metamaterials [21,22], waveguides near the cutoff frequency [23,24], or photonic crystals [25,26]. However, all these resonance-based approaches have the inherent shortcomings in controlling bandwidth and material loss [1,2,27], which nearly rule out any practical potential. There are several enlightening approaches to circumvent the narrow bandwidth issue [28,29], for example, by applying one-dimensional photonic crystals to emulate an epsilon-near-zero medium. It is highly desired to find a different and efficient design framework for this special category of metamaterials by surmounting the existing limitations. In this Letter, we solve these problems by transmuted the material singularities ($n \approx 0$) using an optical conformal mapping (OCM) and build an equivalent

isotropic medium made of normal dielectrics, which is called a near-zero-index-featured (NZIF) structure. A paradigm of electromagnetic (EM) energy tunneling waveguide is introduced to clarify the conception. Applying the OCM scheme [30–33], we show that the material singularity can be eliminated; i.e., the ultralow refractive index of the original NZI media can be vastly increased by several orders to reach superunit values, thus offering high practical feasibility. The quasistatic character of the fields inside the NZIF structure is preserved from the NZI medium during the OCM, which ensures the tunneling effect. The broadband and robustness features of the equivalent waveguide in tunneling EM waves are numerically elaborated in arbitrarily deformed geometries with and without structural defects. The optical transformation provides a promising way to realize NZI-medium-inspired novel devices, which mostly have been deemed impossible in practice [1,2].

A brief flow chart is drawn in Figs. 1(a)–1(c) to illustrate the key ideas on how to transmute the material singularity (refractive index $n \approx 0$) of a NZI-medium-filled waveguide with normal dielectrics in two mathematical steps. The original NZI-medium-based tunneling waveguide, as shown in Fig. 1(a), typically consists of one arbitrary shaped NZI medium (purple region) in between two air-filled rectangular waveguides (cyan region). In the first step, as shown in Fig. 1(b), a suitable conformal

transformation is selectively applied to the main part of the tunneling waveguide so that the middle NZI medium is transformed into a mu-near-zero (MNZ) medium (yellow region) with the relative permittivity $\epsilon_r = 1$ and relative permeability $\mu_r \approx 0$, while the connecting portions of the air-filled waveguides in vicinity of the NZI medium are transformed simultaneously into the OCM adaptors (green region) with the rest unchanged (cyan region). In the second step, as shown in Fig. 1(c), the height of the yellow region is significantly diminished and, as a result, the MNZ medium is transmuted and simply replaced by air. After these two step operations, the original NZI waveguide is successfully transformed into an equivalent device but filled with normal dielectrics (i.e., $\epsilon_r \geq 1$ and $\mu_r = 1$) without influencing waveguide transmission efficiency. The underlying physics will be addressed in detail later. Figure 1(d) gives one simulated result for waves traveling inside the NZIF waveguide, which confirms that our air-filled subwavelength channels can also perfectly tunnel EM waves without reflection. An enlarged picture for the NZIF medium intentionally with some defects is given in Fig. 1(e), which clearly reflects that our NZIF structure is immune to the disturbance of some structural imperfections, as previously observed in the NZI medium [1]. This novel phenomenon, i.e., electromagnetic wave tunneling

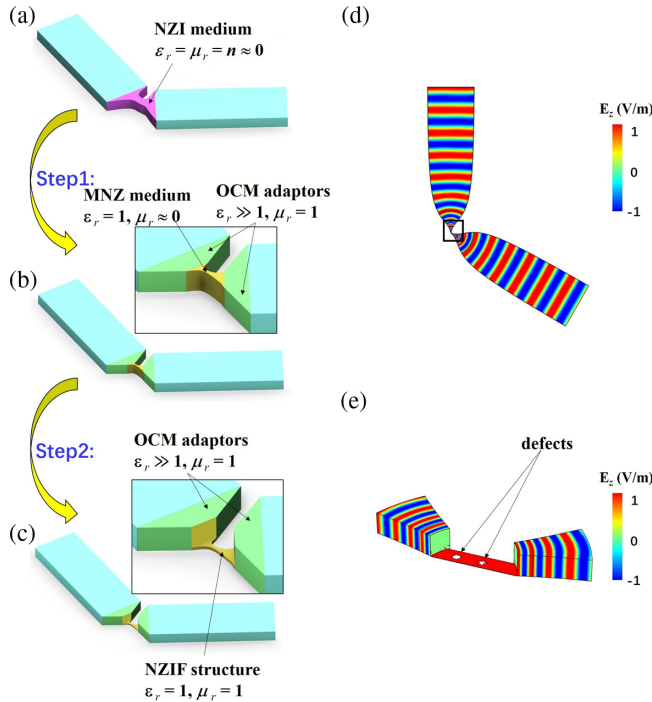


FIG. 1. (a) Conventional NZI-medium-based tunneling waveguide. (b) Obtain the MNZ medium and adaptors from (a) by the OCM. (c) Obtain the NZIF structure by reducing the height of the MNZ medium. (d) Top view of the normalized electric field distribution inside the tunneling waveguide with the NZIF structure. (e) Enlarged plot of the NZIF medium with the PMC defects. The defects are randomly chosen and placed here.

without material singularity ($n \approx 0$) by nonmagnetic normal dielectric, has not been explored before.

For the first step in the above flow chart, we adopt the two-dimensional (2D) Zhukovski mapping as the coordinate transformation [34–39], which can give rise to isotropic permittivity without changing the in plane permeability of transverse electric (TE) waves,

$$\xi = \zeta + \frac{a^2}{\zeta} \quad \text{or} \quad \zeta = \frac{1}{2} \left(\xi \pm \sqrt{\xi^2 - 4a^2} \right), \quad (1)$$

where the complex coordinates $\zeta = x + iy$ and $\xi = u + iv$ denote the coordinates in the physical and reference space, respectively. Zhukovski mapping can transform the branch cut, i.e., blue line segments in Fig. 2(a), into a blue circle with radius of a in Fig. 2(b). Correspondingly, the double Riemann sheets in the reference space are also transformed into the interior and exterior domains of the transformed branch cut in the physical space [30,40]. After the mapping, the original dielectric property ϵ_ξ will be transformed and in the physical space can be rewritten by ϵ_ζ ,

$$\epsilon_\zeta = M^2(\zeta) \cdot \epsilon_\xi, \quad (2)$$

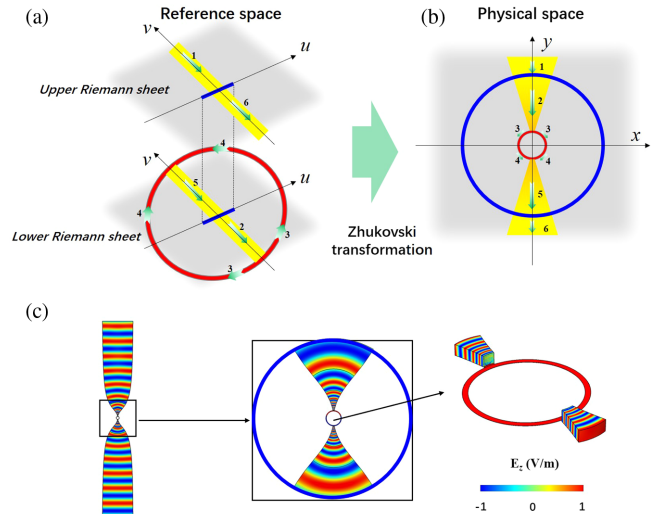


FIG. 2. (a),(b) The basic idea of promoting the relative permittivity of NZI medium to one with Zhukovski transformation. (a) A NZI medium ($\epsilon_r = \mu_r = 10^{-4}$) (colored in red) connects two air-filled waveguides (colored yellow) in the reference space. (b) The corresponding transformed structures by Zhukovski mapping in the physical space. The MNZ medium ($\epsilon_r \geq 1$, $\mu_r = 10^{-4}$) and OCM adaptors ($\epsilon_r \geq 1$, $\mu_r = 1$) are colored in red and yellow, respectively. Note regions with the same color in the reference space and physical space have different material parameters. (c) The electric field distributions inside the NZIF-based waveguide in the physical space by numerical simulation. The wavelength is set to $\lambda_0 = a$. The right two insets are the enlarged plots. The blue circle is the corresponding “branch cut” in the physical space.

where the multiplier factor $M(\zeta)$ for Zhukovski mapping is defined as

$$M(\zeta) = \left| 1 - \frac{a^2}{\zeta^2} \right|, \quad (3)$$

which is determined by the length of the branch cut a and the positions in the complex coordinates. The transformation details are described in Figs. 2(a) and 2(b). The NZI medium is transformed to MNZ medium and the air-filled waveguides are transformed to OCM adaptors. The green arrows in both the reference space and physical space indicate the Poynting energy flow with numbers representing the time sequence. The boundaries of the waveguides are a perfect magnetic conductor (PMC) for TE waves, which are invariant during the transformation. Gray rest regions outside the waveguide are treated as air as they do not influence the waveguide modes. Note that the in plane relative permeability ($\mu_r \approx 0$) for TE waves is not changed during the OCM [31].

For the second step in the flow chart, nonmagnetic materials are used to replace the above MNZ medium, and scattering at the interfaces will happen due to the impedance mismatch. As proved later, this issue could be elegantly solved by reshaping the physical dimensions of the NZIF structure. The only sacrifice is that the device structure will be evolved from the original 2D design into a three-dimensional (3D) one by introducing a small-gapped parallel-plate waveguide as shown in Figs. 1(b) and 1(c). The electric field distribution in the physical space is shown in Fig. 2(c), which shows the subwavelength circular NZIF structure can tunnel EM waves. The NZIF structure can be designed with more flexibility, e.g., arbitrary shape and orientation. Details can be found in the first part of the Supplemental Material [41].

Here, both NZI- and NZIF-based channels can tunnel EM waves but with different mechanisms. Conventional NZI-medium-based channels can transmit EM waves due to its material singularity ($n \approx 0$), while the NZIF-structure-based channels have the same function due to their structural singular properties, i.e., with the physical dimensions approaching zero. Both material and structural singularities can lead to the quasistatic character of the fields inside the channel. In other words, the effective local wavelength is infinitely large compared with the size of the tunneling channel. From the view of transformation optics, the above two tunneling mechanism are unified; i.e., material parameters and the spatial geometries have the same impact on waves and fields.

The mechanism of the above designed NZIF-based waveguide can be well explained physically by transmission line circuit theory or by directly solving Maxwell equations inside the waveguide. For the key portion of the NZIF waveguide as draw in Fig. 3(a), a simple transmission line circuit can be first used to

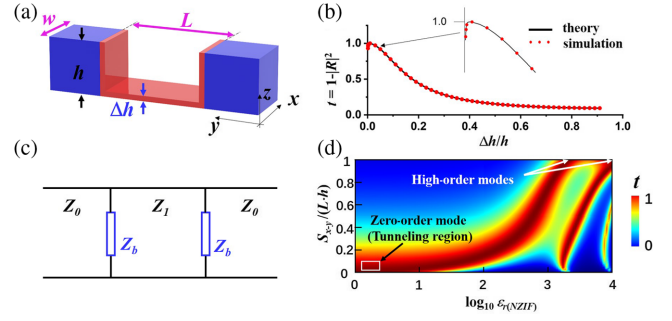


FIG. 3. (a) A 3D structure model of the OCM adaptor and NZIF structure, similar to Fig. 1(e) without defects. (b) Power transmission coefficient t with respect of the normalized height $\Delta h/h$. Blue curve is the theory calculation and the red dot is the numerical simulation result. (c) Transmission line model of the OCM adaptor and NZIF structure. (d) Power transmission coefficient t with respect of the normalized cross-sectional area $S_{y-z}/(Lh)$ and the relative permittivity of the NZIF structure. We choose $h = 1/200\lambda_0$ and $L = 1/100\lambda_0$ for (b) and (d).

qualitatively address the tunneling effect, as plotted in Fig. 3(c) where Z_0 (Z_1) and Z_b are the characteristic impedance of the OCM adaptor (the NZIF structure) and the boundary impedance, respectively. The characteristic impedance inside the rectangular waveguide can be expressed as $Z = \sqrt{(\mu/\epsilon)}(h/w)$, where μ , ϵ , h , and w are the permeability, permittivity, height, and width of the waveguide, respectively. As the permittivity inside the OCM region is far larger than that inside the NZIF structure, we can substantially reduce the height of the NZIF portion to match Z_0 and Z_1 . To minimize the boundary effect, we need to add two ultrathin NZIF layers of the same height with the OCM adaptor at the two ends, thus effectively forming a U-shaped cross section for the whole NZIF region as plotted in Fig. 3(a). According to this design, the two thin NZIF layers have the same height with the OCM adaptor but much smaller permittivity ($\epsilon_r = 1$), which will contribute to an infinite relative boundary impedance [42], i.e., $Z_b \gg Z_0$ (or Z_1). Therefore, the incoming wave will not perceive the structural discontinuity and transmit forward without reflection as the impedance is matched everywhere.

The tunneling effect can also be well explained physically from the mode distribution inside the waveguide by solving the Maxwell equations with boundary conditions. For the structure in Fig. 3(a), the reflection coefficient can be deduced as (details can be found in the second part of the Supplemental Material [41])

$$R = \frac{\Delta h \epsilon_r k_0 S_{y-z} - h^2 k_0 L}{2ih\Delta h \sqrt{\epsilon_r} + \Delta h \epsilon_r k_0 S_{y-z} + h^2 k_0 L}, \quad (4)$$

where k_0 is the free space wave vector, and ϵ_r is the effective relative permittivity of the OCM adaptors (near the U-shaped NZIF structure). $S_{y-z} = \Delta h \cdot (L + 2h - 2\Delta h)$

is the cross-sectional area of the NZIF structure in the $y-z$ plane, h is the height of the OCM adaptors, Δh and L are the height and length of the NZIF structure [see Fig. 3(a)]. Equation (4) shows that the reflection coefficient is strictly zero if $\Delta h = \sqrt{(L/L + 2h)(h/\sqrt{\epsilon_r})}$. Actually, the reflection coefficient can be small enough when Δh is on the order of $h/\sqrt{\epsilon_r}$ (the impedance matched case deduced by the above transmission line theory), where $|R| = 2\pi h/\lambda_0 \approx 0$ (λ_0 is the wavelength of free space). $|R|^2$ is less than 0.1 in Fig. 1(d) calculated by Eq. (4), which ensures a good tunneling effect.

The power transmission coefficient $t = 1 - |R|^2$ with varied Δh is shown in Fig. 3(b). The theory calculation (black curve) using Eq. (4) fits well with the numerical simulations (red dots), which confirms the validity of eliminating the reflection by reducing the height of the NZIF structure. Note that when $\Delta h < \sqrt{(L/L + 2h)(h/\sqrt{\epsilon_r})}$, the power transmission coefficient drops rapidly to zero (with $\Delta h \rightarrow 0$) as large impedance mismatch occurs. If the relative permittivity of the NZIF structure is much larger than 1, Eq. (4) cannot give a precise description, as the quasistatic approximation is no longer satisfied. To get a comprehensive understanding of the tunneling effect, we use 2D numerical simulations to obtain the power transmission coefficient with varied relative permittivity of the NZIF structure $\epsilon_{r(\text{NZIF})}$ and its cross-sectional area in $y-z$ plane S , which is shown in Fig. 3(d). The x axis represents the logarithmic form of $\epsilon_{r(\text{NZIF})}$. The y axis represents the normalized cross-sectional area in the $y-z$ plane of the NZIF region, i.e., $S_{y-z}/(Lh)$. The bottom left region inside the white rectangle is the NZIF region, which correspond to the zero-order mode, where EM energy can tunnel through the channel with a constant phase. When S_{y-z} increases, some other modes with different relative permittivity can also have a large transmittance, which corresponds to the high-order modes. However, these high-order modes are frequency dependent and cannot work in a broad bandwidth. Note that the waves inside the OCM adaptor are reflectionless due to the continuous change of the relative permittivity, which is transformed from empty space by Zhukovski mapping. Therefore, the whole waveguide can guide TEM waves without reflection.

The NZIF structure is not sensitive to some kinds of structural defects randomly distributed inside the NZIF structure. When defects are immersed in the NZIF region, the reflection coefficient can be written as (details can be found in the third part of the Supplemental Material [41])

$$R = \frac{-i\pi(s + \frac{E_d}{E_z}\epsilon_d s_d)}{w\lambda_0 + i\pi(s + \frac{E_d}{E_z}\epsilon_d s_d)}, \quad (5)$$

where E_d is the average value of the electric fields inside the defects, and E_z is the electric fields outside the defects

at the bottom of the U-shaped NZIF structure. s and s_d are the cross-sectional area of the NZIF structure and the defects in the $x-y$ plane, respectively. ϵ_d is the relative permittivity of the defects, λ_0 is the free space wavelength, and w is the width (x direction) of the NZIF structure. If the defects are perfect electric conductor (PEC) objects, both E_z and E_d tend to zero; however, their ratio is still a finite number and is far smaller than the absolute value of the permittivity $\epsilon_d [\approx \text{Im}\sigma/(\epsilon_0\omega)]$ and is an infinitely large imaginary number, i.e., $|\epsilon_d| \gg |E_z/E_d|$, therefore $w\lambda_0$ can be ignored, and for this case, $R = -1$; i.e., waves are totally reflected, which is shown in Fig. 4(b). If the defects are PMC objects, E_d vanishes, E_z is a finite number, and the reflection coefficient tends to zero because λ_0 is much larger than the width (w) and the length (L) of the NZIF structure; i.e., tunneling effect is not influenced by the PMC defects with arbitrary sizes, shapes, and positions. As shown in Fig. 4(a), circular and pentagram-shaped PMC defects are embedded in the NZIF structure, which have almost no influence on the tunneling effect. For other dielectric and magnetic defects, E_d is comparable with E_z , and both Eq. (5) and numerical simulations show that the tunneling effect is not disturbed with magnetic defects or weak dielectric defects. However, the tunneling effect gets worse if the relative permittivity of dielectrics defects gets larger, see Figs. 4(c)–4(f).

Because both the NZIF structure and the OCM adaptors are made of normal dielectrics, the device will have broadband and low loss features. Detailed discussions about the broadband feature and comparison with conventional NZI-based tunneling waveguide can be found in Figs. S4 and S5 in the Supplemental Material [41]. Regarding the implementation, the key component is for the OCM adaptor made of gradient refractive index materials, which, in principle, can be realized by artificial composites, e.g., ceramic blocks with different permittivity. The maximum permittivity in our design is 10000, which is

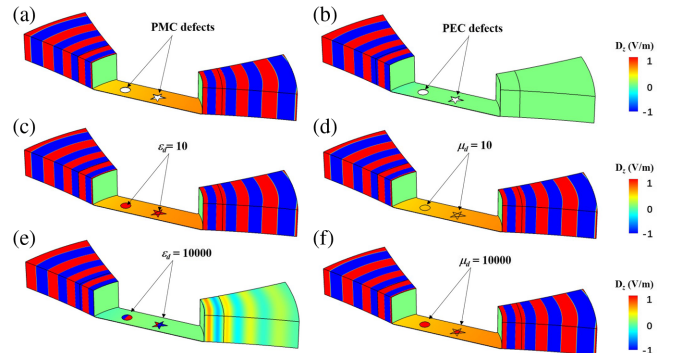


FIG. 4. Electric displacement distribution of the tunneling waveguide with defects-embedded-NZIF structures. (a) PMC defects. (b) PEC defects. (c) Dielectric defects with $\epsilon_d = 10$. (d) Magnetic defects with $\mu_d = 10$. (e) Dielectric defects with $\epsilon_d = 10000$. (f) Magnetic defects with $\mu_d = 10000$. ϵ_d and μ_d are the relative permittivity and permeability of the defects.

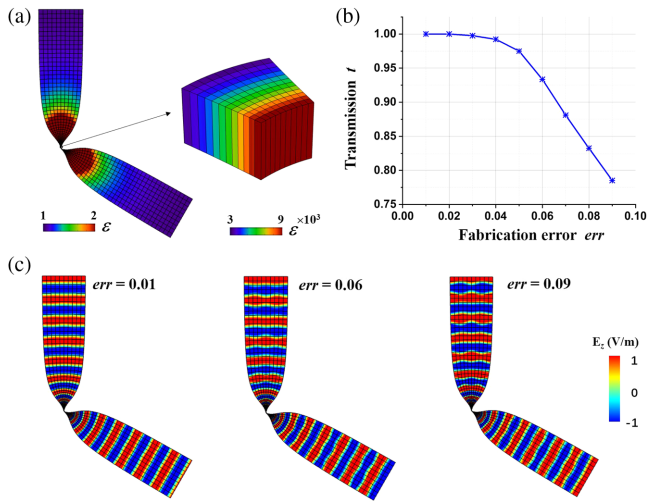


FIG. 5. Realization by ceramic blocks with different permittivity. (a) Permittivity distribution of the unit cells. (b) Power transmission coefficient against the fabrication error. (c) Electric field distributions of the tunneling waveguide with different fabrication errors.

available in reality, e.g., barium titanate in the microwave region [43]. Square-shaped unit cells with side length about $1/5$ local effective wavelength are chosen here for practical realization (no variation in z direction). Each unit cell is filled with uniform dielectrics with different permittivity, as shown in Fig. 5(a). The tunneling effect is nearly perfect with these unit cells. For real application, fabrication errors may influence the tunneling effect. Here, random noise of the refractive index is added to each unit cell to check the fabrication tolerance of the tunneling waveguide. To do this, the refractive index is modified by $n_{\text{modified}} = n_{\text{original}}(1 + \text{err})$ for each unit cell, where “err” is the random noise ratio representing the fabrication uncertainty. Figure 5(b) shows the power transmission coefficient against the fabrication error. Three corresponding electric field distribution with different noise ratios ($\text{err} = 0.01, 0.06, \text{ and } 0.09$) are shown in Fig. 5(c). The results show that prominent tunneling effect can be obtained with $\text{err} < 0.06$, where the power transmission coefficient is larger than 0.93. Therefore, the tunneling waveguide is robust against fabrication errors, i.e., within about 6% fabrication error.

In conclusion, we propose a rigorous method to realize the NZI medium with a material-singularity-transmuted configuration, i.e., NZIF structure with its refractive index above 1. As an illustrative case, the broadband subwavelength EM wave tunneling effect with NZIF structure is verified. Numerical simulations show that the designed NZIF medium can tunnel EM energy through subwavelength channels between waveguides. The robustness of the design is also numerically proved against some structural defects inside the subwavelength channels. The EM energy tunneling waveguide by NZIF structure can be realized by normal dielectrics with relative permittivity above 1, which

shows broad bandwidth and low loss features and, hence, improves the performance of the EM energy tunneling waveguides by NZI medium. The proposed method can also be extended to improve the bandwidth and performance of other conventional NZI-based devices by using normal dielectrics with high relative permittivity.

This work is partially supported by the National Natural Science Foundation of China (Nos. 61905208, 61971300, 61775195, 62075196, and 11674239), Scientific and Technological Innovation Programs (STIP) of Higher Education Institutions in Shanxi (Nos. 2019L0146 and 2019L0159), the National Key Research and Development Program of China (No. 2017YFA0205700), and the Fundamental Research Funds for the Central Universities.

The authors declare no competing financial interests.

*sunfei@tyut.edu.cn

†yungui@zju.edu.cn

- [1] I. Liberal and N. Engheta, Near-zero refractive index photonics, *Nat. Photonics* **11**, 149 (2017).
- [2] N. Kinsey, C. DeVault, A. Boltasseva, and V.M. Shalae, Near-zero-index materials for photonics, *Nat. Rev. Mater.* **4**, 742 (2019).
- [3] D. C. Adams, S. Inampudi, T. Ribaldo, D. Slocum, S. Vangala, N. A. Kuhta, W. D. Goodhue, V. A. Podolskiy, and D. Wasserman, Funneling Light through a Subwavelength Aperture with Epsilon-near-Zero Materials, *Phys. Rev. Lett.* **107**, 133901 (2011).
- [4] M. Silveirinha and N. Engheta, Tunneling of Electromagnetic Energy through Subwavelength Channels and Bends Using Epsilon-near-Zero Materials, *Phys. Rev. Lett.* **97**, 157403 (2006).
- [5] D. A. Powell, A. Alu, B. Edwards, A. Vakil, Y. S. Kivshar, and N. Engheta, Nonlinear control of tunneling through an epsilon-near-zero channel, *Phys. Rev. B* **79**, 245135 (2009).
- [6] R. Liu, Q. Cheng, T. Hand, J. J. Mock, T. J. Cui, S. A. Cummer, and D. R. Smith, Experimental Demonstration of Electromagnetic Tunneling through an Epsilon-near-Zero Metamaterial at Microwave Frequencies, *Phys. Rev. Lett.* **100**, 023903 (2008).
- [7] A. Ourir, A. Maurel, and V. Pagneux, Tunneling of electromagnetic energy in multiple connected leads using is an element of near-zero materials, *Opt. Lett.* **38**, 2092 (2013).
- [8] S. Campione, J. R. Wendt, G. A. Keeler, and T. S. Luk, Near-infrared strong coupling between metamaterials and epsilon-near-zero modes in degenerately doped semiconductor nanolayers, *ACS Photonics* **3**, 293 (2016).
- [9] M. G. Silveirinha and N. Engheta, Theory of supercoupling, squeezing wave energy, and field confinement in narrow channels and tight bends using e near-zero metamaterials, *Phys. Rev. B* **76**, 245109 (2007).
- [10] M. G. Silveirinha, Trapping light in open plasmonic nanostructures, *Phys. Rev. A* **89**, 023813 (2014).

- [11] F. Monticone, H. M. Doeleman, W. Den Hollander, A. F. Koenderink, and A. Alu, Trapping light in plain sight: Embedded photonic eigenstates in zero-index metamaterials, *Laser Photonics Rev.* **12**, 1700220 (2018).
- [12] S. Enoch, G. Tayeb, P. Sabouroux, N. Guerin, and P. Vincent, A Metamaterial for Directive Emission, *Phys. Rev. Lett.* **89**, 213902 (2002).
- [13] R. W. Ziolkowski, Propagation in and scattering from a matched metamaterial having a zero index of refraction, *Phys. Rev. E* **70**, 046608 (2004).
- [14] H. Zhou, Z. Pei, S. Qu, S. Zhang, J. Wang, Q. Li, and Z. Xu, A planar zero-index metamaterial for directive emission, *J. Electromagn. Waves Appl.* **23**, 953 (2009).
- [15] H. X. Xu, G. M. Wang, and T. Cai, Miniaturization of 3-D anisotropic zero-refractive-index metamaterials with application to directive emissions, *IEEE Trans. Antennas Propag.* **62**, 3141 (2014).
- [16] T. Cao, Y. Zou, A. M. Adawi, and M. J. Cryan, Directive emission of red conjugated polymer embedded within zero index metamaterials, *Opt. Express* **22**, 22699 (2014).
- [17] M. Z. Alam, I. De Leon, and R. W. Boyd, Large optical nonlinearity of indium tin oxide in its epsilon-near-zero region, *Science* **352**, 795 (2016).
- [18] L. Caspani *et al.*, Enhanced Nonlinear Refractive Index in Epsilon-near-Zero Materials, *Phys. Rev. Lett.* **116**, 233901 (2016).
- [19] C. Argyropoulos, P. Y. Chen, G. D'Aguanno, N. Engheta, and A. Alu, Boosting optical nonlinearities in epsilon-near-zero plasmonic channels, *Phys. Rev. B* **85**, 045129 (2012).
- [20] C. Argyropoulos, G. D'Aguanno, and A. Alu, Giant second-harmonic generation efficiency and ideal phase matching with a double epsilon-near-zero cross-slit metamaterial, *Phys. Rev. B* **89**, 235401 (2014).
- [21] G. Subramania, A. J. Fischer, and T. S. Luk, Optical properties of metal-dielectric based epsilon near zero metamaterials, *Appl. Phys. Lett.* **101**, 241107 (2012).
- [22] X. D. Yang, C. Y. Hu, H. X. Deng, D. Rosenmann, D. A. Czaplewski, and J. Gao, Experimental demonstration of near-infrared epsilon-near-zero multilayer metamaterial slabs, *Opt. Express* **21**, 23631 (2013).
- [23] A. M. Mahmoud and N. Engheta, Wave-matter interactions in epsilon-and-mu-near-zero structures, *Nat. Commun.* **5**, 5638 (2014).
- [24] C. Della Giovampaola and N. Engheta, Plasmonics without negative dielectrics, *Phys. Rev. B* **93**, 195152 (2016).
- [25] X. Q. Huang, Y. Lai, Z. H. Hang, H. H. Zheng, and C. T. Chan, Dirac cones induced by accidental degeneracy in photonic crystals and zero-refractive-index materials, *Nat. Mater.* **10**, 582 (2011).
- [26] P. Moitra, Y. M. Yang, Z. Anderson, II. Kravchenko, D. P. Briggs, and J. Valentine, Realization of an all-dielectric zero-index optical metamaterial, *Nat. Photonics* **7**, 791 (2013).
- [27] J. B. Khurgin, How to deal with the loss in plasmonics and metamaterials, *Nat. Nanotechnol.* **10**, 2 (2015).
- [28] K. Konstantinidis and A. P. Feresidis, Broadband near-zero index metamaterials, *J. Opt.* **17**, 105104 (2015).
- [29] V. Popov, S. Tretyakov, and A. Novitsky, Brewster effect when approaching exceptional points of degeneracy: Epsilon-near-zero behavior, *Phys. Rev. B* **99**, 045146 (2019).
- [30] U. Leonhardt, Optical conformal mapping, *Science* **312**, 1777 (2006).
- [31] L. Xu and H. Y. Chen, Conformal transformation optics, *Nat. Photonics* **9**, 15 (2015).
- [32] Y. G. Ma, C. K. Ong, T. Tyc, and U. Leonhardt, An omnidirectional retroreflector based on the transmutation of dielectric singularities, *Nat. Mater.* **8**, 639 (2009).
- [33] Y. G. Ma, F. Sun, Y. Zhang, Y. Jin, and C. Ong, Approaches to achieve broadband optical transformation devices with transmuted singularity, *J. Opt. Soc. Am. A* **29**, 124 (2012).
- [34] J. B. Pendry, D. Schurig, and D. R. Smith, Controlling electromagnetic fields, *Science* **312**, 1780 (2006).
- [35] F. Sun, B. Zheng, H. S. Chen, W. Jiang, S. W. Guo, Y. C. Liu, Y. G. Ma, and S. L. He, Transformation optics: From classic theory and applications to its new branches, *Laser Photonics Rev.* **11**, 1700034 (2017).
- [36] Y. C. Liu, F. Sun, and S. L. He, Omnidirectional Conformal Cloak Without Geometrical Dispersion, *Phys. Rev. Appl.* **12**, 064009 (2019).
- [37] Y. C. Liu, F. Sun, and S. L. He, Controlling lightwave in Riemann space by merging geometrical optics with transformation optics, *Sci. Rep.* **8**, 514 (2018).
- [38] Y. C. Liu, M. Mukhtar, Y. G. Ma, and C. K. Ong, Transmutation of planar media singularities in a conformal cloak, *J. Opt. Soc. Am. A* **30**, 2280 (2013).
- [39] Y. G. Ma, Y. C. Liu, L. Lan, T. T. Wu, W. Jiang, C. K. Ong, and S. L. He, First experimental demonstration of an isotropic electromagnetic cloak with strict conformal mapping, *Sci. Rep.* **3**, 2182 (2013).
- [40] Y. G. Ma, T. T. Wu, and C. K. Ong, Subwavelength drains designed for mirror-closed dielectric lenses, *J. Opt.* **15**, 125705 (2013).
- [41] See Supplemental Material at <http://link.aps.org/supplemental/10.1103/PhysRevLett.125.207401> for details about the flexible design of the NZIF structure, the derivation of the reflection coefficient of the NZIF structure with and without defects, and the numerical simulations of the broadband feature of the tunneling waveguide.
- [42] R. E. Collin, *Field Theory of Guided Waves*, 2nd ed. (IEEE Press, New York, 1990).
- [43] T. Karaki, K. Yan, and M. Adachi, Barium titanate piezoelectric ceramics manufactured by two-step sintering, *Jpn. J. Appl. Phys.* **46**, 7035 (2007).